International Journal of Power Electronics and Drive System (IJPEDS)
Vol. 16, No. 2, June 2025, pp. 1230~1247
ISSN: 2088-8694, DOI: 10.11591/ijpeds.v16.i2.pp1230-1247

Performance analysis of an islanded variable speed wind energy system during multi-mode operation

P. Preethi Santhosam[1], U. Sowmmiya[1], Tole Sutikno[2,3]
[1]Department of Electrical and Electronics Engineering, SRM Institute of Science and Technology, Chennai, India
[2]Department of Electrical Engineering, Faculty of Industrial Technology, Universitas Ahmad Dahlan, Yogyakarta, Indonesia
[3]Embedded System and Power Electronics Research Group, Yogyakarta, Indonesia

Article Info

Article history:

Received Feb 18, 2025
Revised May 1, 2025
Accepted May 19, 2025

Keywords:

DFIG
Islanded operation
Multimode power transfer
Oscillations
Wind energy system

ABSTRACT

Unbalances and non-linearities in islanded wind energy systems (WES) cause electromagnetic torque fluctuations, leading to mechanical stress and power oscillations. This study analyses the dynamic performance of a doubly fed induction generator (DFIG)-based variable speed WES connected to a standalone DC microgrid (DCM) during multimode operations. The proposed system addresses power balance during rare scenarios such as machine stall, closed rotor, and closed stator conditions. Notably, only one stator parameter regulates voltage and frequency, simplifying control and reducing cost. Unlike existing literature, this work quantifies and demonstrates the oscillations in torque, active, and reactive power. Dynamic performance is validated using a software-in-loop (SIL) approach with the Opal RT OP4510 real-time simulator. Results confirm that the system maintains voltage stability and supports uninterrupted power delivery across all operational modes. Additionally, power quality indices such as THD comply with IEEE 519 standards, reporting system reliability and flexibility in standalone wind energy applications.

Corresponding Author:

U. Sowmmiya
Department of Electrical and Electronics Engineering, SRM Institute of Science and Technology, Kattankulathur, Chennai 603203, Tamil Nadu, India
Email: sowmmeee@gmail.com

1. INTRODUCTION

The global increase in energy demand and the fast depletion of fossil fuels necessitate the addition of new renewable sources into the utility with reliability in supply. Wind power exists as a promising source of energy on account of increased unit capacity, increased power production with erratic wind input, and also due to the performance-price ratios of generators. The doubly fed induction generator (DFIG) is the crucial member of a variable speed wind generator and exerts slip power recovery. It mainly concentrates on the maximum extraction and utilization of power from wind under all conditions [1], [2]. Owing to the heavy integration of renewables, many smaller grids of both AC and DC in nature are coupled together to frame hybrid AC/DC networks, thereby enabling islanded and grid-tied operations [3]. In this work, the variable speed DFIG-based wind energy system (WES) is connected to a hybrid AC/DC network, enabling islanded operation and grid-tied operation. However, an islanded system is so fragile and necessitates a disturbance or oscillation study on account of any system disturbance/ unbalances/non-linearity. Hence, this work focuses on the oscillations' occurrence and power transfer during the multimode operation of WES.

In any islanded WES, the regulation of system parameters is a challenging task. Furthermore, an islanded system must be robust to active wind velocity and load variations [4], [5]. The WES, when subjected to disturbances or unbalances/non-linearity, the system encounters oscillations. Due to which the

electromagnetic torque also exerts oscillations, causing mechanical stress, thereby leading to a reduction in efficiency and wear and tear of the machine. Also, the oscillations keep spreading to the vital parameters such as current and power. As per Indian Grid Codes, the WES should comply with reducing the oscillations well less than the recommended limits [6], [7]. Unlike the other reported literature, this work reports the oscillations that occur in currents, torque, and power when the system is subjected to unbalance and nonlinearity.

Most of the literature reports two back-to-back converters for any isolated DFIG-based WECS [8], demanding control for both converters separately, leading to increased system cost and control complexity. In this work, only one converter, which is the rotor side converter [RSC], is considered. The rotor side converter (RSC) is typically rated at only 30–40% of the total system capacity, which contributes to a reduction in overall system cost. Various control strategies have been explored for managing the RSC, including direct torque control, field-oriented control, and advanced nonlinear approaches such as sliding mode and slip control. Studies [9]–[11] have addressed the dynamic modeling and implementation of decoupled current control for DFIG-based wind energy systems under grid disturbances. An improved sliding mode control is discussed in [12], [13] to evade the system disturbances and attain greater stability during nonlinear conditions. Vector-based predictive direct power control is discussed in [14] to predict the future power slot by keeping the current power slot, leading to multiple computations and storage of current data. The combination of direct power control with field-oriented control, as proposed in [15], [16], imposes reliability on active and reactive power but produces a sluggish response during dynamic system parameter changes. A simple traditional proportional-integral (PI) controller implemented in [17], [18] analyzes the disturbances and controls the stability issues, but lacks responses. The multi-source operation of a micro-grid with a control plan is discussed in [19], [20] involves mathematical manipulation leading to control complexities on real-time implementation. Few micro-grids are operated with batteries for stability purposes [21], but they all suffer from charging limitations. The aforementioned control techniques for DFIG comprise mathematical modeling, sensing, parameter estimation, and sophisticated instrumentation. Also, this literature reports the efficacy of the control scheme only during normal operations and fails to transfer power during any adverse conditions. A comparison schematic of the afore-mentioned literature and the proposed work is depicted in Figure 1.

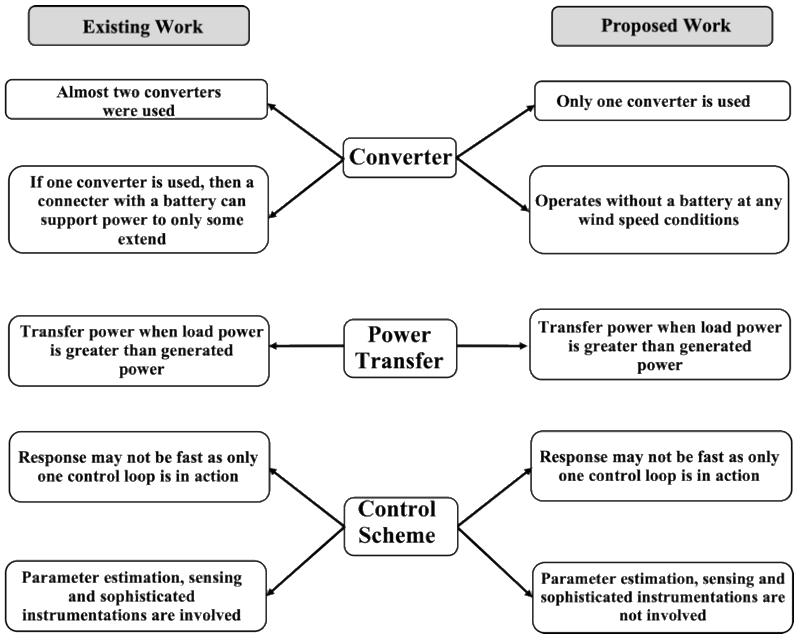

Figure 1. Comparison schematic of the afore-mentioned literature and the proposed work

In the present work, the various possible multi-modes of operation and the dynamic performance of islanded DFIG-based WES coupled to a DC microgrid are proposed. It can be operated during various load/wind speed conditions. The exceptional modes, such as machine stall, and rotor and stator closed circuit [CR-CS], are significantly analyzed for verifying the system's flexibility to operate in all possible conditions. At the time of closed-circuit condition in the windings, DFIG behaves as a cage machine, either as closed rotor (CR) or a closed stator (CS). When subjected to any DCM voltage reduction then the CS mode will be triggered. The principal intent of the work is to provide an efficient power transfer during potential multimode current-

controlled RSC. Also, an oscillation occurrence analysis in comparison with certain reported literature analysis is exhibited when the system is subjected to unbalance and non-linearity in loads during its islanded operation. To put forth the islanded mode by maintaining the stator voltage and frequency through RSC, a decoupled, cascaded voltage-current control is adopted. It also enables the system to withstand the system dynamics with minimal overshoot. A software-in-loop (SIL) approach through Opal RT (OP4510) based real-time controller is adopted to validate the system, and the results symbolize bidirectional slip power transfer, stator voltage and frequency regulation, and multimode power transfer operations. Also, it is observed that the oscillations prevail during the dynamic operations on the rotor parameters and electromagnetic torque, which might exhibit oscillations on the stator, thereby a stress on the machine. The oscillations are quantified and reported in this work. The main contributions of the paper are:

- Detailed design and modeling of system components;
- Implementation of decoupled cascaded current control for RSC only – The system involves only one converter, and that is rated only to about 30-40% [Uses only one stator parameter for the regulation of the system];
- System versatility – Delivers uninterrupted power supply even during inadvertent conditions such as machine stall and closed-circuit conditions; and
- Reduction of oscillations during unbalance and non-linearity as compared to other reported literature.

This paper is structured as follows: i) Section 2 outlines the system architecture and its components; ii) Section 3 presents the system modeling and design methodology; iii) Section 4 describes in detail the control scheme adopted to exert the possible power transfer modes; iv) Section 5 presents the system evaluation based on its performance through software-in-loop approach; and v) Section 6 outlines the conclusions drawn out of the work reported in this paper.

2. CONFIGURATION OF THE WES

The variable speed DFIG-based WES tied to the DC microgrid (DCM) is depicted in Figure 2. The renewables, such as solar photovoltaic, DC-powered electric vehicle (EV), and energy storage systems, frame the DCM. A battery is integrated with the DC microgrid (DCM) to enable bidirectional power flow, allowing it to store surplus energy and supply power during shortages or faults in the DCM, thereby enhancing system reliability. However, the sources connected to the DC end are for depiction purposes only. The stator end of DFIG is connected to a point of intersection [PoI] where unbalanced and nonlinear loads are also coupled, making the system voltages and currents more distorted and unbalanced. Also, the presence of unbalance and non-linearity in loads at the stator causes oscillations in power and torque, framing the prime aim of this study. To curb the oscillations and to exhibit regulation of system parameters, a rotor side converter [RSC], which is a 3ϕ, three-leg, current-controlled, bidirectional, PWM-based voltage source converter [PWM-VSI] is employed in the WES. It is designed to facilitate bidirectional slip power transfer within the system using PWM-based rectification and inversion. The RSC is connected through feeder impedances to reduce the oscillations that arise due to harmonics and any single phasing. During excess power generation, the generated power is fed to DCM through the process of PWM rectification. During a deficit of power production from DFIG, the DCM would support the power supply to loads through the process of PWM inversion. The WES proposed in this study exhibits multi-mode operation depending on the wind velocity and load conditions. The various formulated modes are normal operation, machine stall, closed circuit [closed stator (CS) and closed rotor (CR)]. Detailed specifications are given in Table 1.

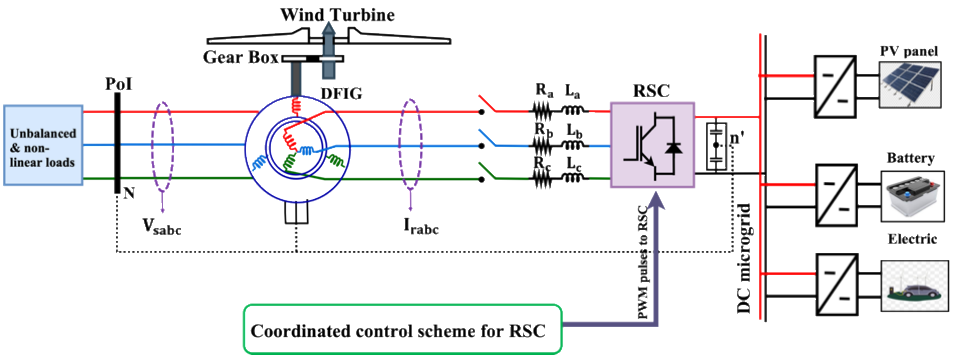

Figure 2. Configuration of the variable speed DFIG based WES

Table 1. System specifications

System specifications	Value
DFIG	Benn make/1.5HP/230 V/3ϕ/4 poles/1500 rpm/R_{st} = 1.405 Ω/ R_r= 1.395 Ω/L_{st} = L_r = 0.005839 H/L_m = 0.1722 H
DC machine	Benn make/2 HP/V_A = V_f = 220 V/I_A= 8 A/I_f = 0.5 A
Load parameters	R_a= 500 Ω, R_b= 450 Ω, R_c = 480 Ω (unbalanced loads) Diode bridge rectifier connected to R = 520 Ω (nonlinear load)
RSC	SEMIKRON makes, SKM100GB12TH IGBT module-based converter DC side voltage: 400 V

3. MODELING AND DESIGN – SYSTEM COMPONENTS

The system under study employs a wind turbine for speed variation, DFIG for power generation, DCM and RSC for bi-directional power flow, and the loads. The modeling and design equations of the system are detailed below.

3.1. Modeling and design of wind turbine and generator

The presence and usability of wind power, P_ω is computed using (1) concerning the area covered by the rotation of wind blades *A*, wind velocity V_ω, ρ is specific air density (ρ = 1.15 kg/m^3), and the turbine's coefficient of power, K_p, which is computed as in (2).

$$P_\omega = \frac{1}{2} K_P \rho A V_\omega^3 \quad (1)$$

$$\left.\begin{aligned} K_p(\lambda,\theta) &= K_1\left\{\left(\frac{K_2}{\lambda_i}\right) - K_3\theta - K_4\right\} e^{\frac{-K_5}{\lambda_i}} + K_6\lambda \\ \lambda &= \frac{\omega_r R_d}{V_\omega} \end{aligned}\right\} \quad (2)$$

Where, pitch angle of the blade of the turbine is represented as θ, and the tip speed ratio is denoted as λ. The tip speed ratio is computed using the rotor speed ω_r, wind velocity V_ω, radius of the rotation that the wind turbine makes, R_d, and the constants K_1-K_6 as in (2) with the values being 0.52, 120, 0.6, 4.77, 23, 0.0056, respectively. In the proposed work, a 1.5 kW DFIG machine is designed to operate with a maximum wind velocity of 15 m/s. The maximum K_p value is presumed to be 0.48 when β = 0 for λ = 8.1 [22], [23].

The DFIG employed in the work is modeled with (3)-(6), presuming a reference frame to be stationary, thereby making the angular speed zero. The voltage equations for the stator and the rotor in the d-q frame are given as (3) and (4).

$$V_{d\_st} = R_s I_{d\_st} + \rho\lambda_{d\_st} - \omega\lambda_{q\_st} \;;\; V_{q\_st} = R_{st} I_{q\_st} + \rho\lambda_{q\_st} + \omega\lambda_{d\_st} \quad (3)$$

$$V_{d\_r} = R_r I_{d\_r} + \rho\lambda_{d\_r} - (\omega - \omega_r)\lambda_{q\_r}; V_{q\_r} = R_r I_{q\_r} + \rho\lambda_{q\_r} + (\omega - \omega_r)\lambda_{d\_r} \quad (4)$$

The flux linkage equations for the stator and the rotor are given in (5) and (6).

$$\varphi_{d\_st} = L_{st} I_{d\_st} + L_m I_{d\_r}; \varphi_{q\_st} = L_{st} I_{q\_st} + L_m I_{q\_r} \quad (5)$$

$$\varphi_{d\_r} = L_m I_{d\_st} + L_r I_{d\_r} \;; \varphi_{q\_r} = L_m I_{q\_st} + L_r I_{q\_r} \quad (6)$$

Where V_{d_st}, V_{q_st} are the two phase components in terms of direct and quadrature (d-q) stator voltages; I_{d_st}, I_{q_st} are the two phase components in terms of direct and quadrature (d-q) stator currents; I_{d_r}, I_{q_r} are the two phase components in terms of direct and quadrature (d-q) stator currents; V_{d_r}, V_{q_r} are the two phase components in terms of direct and quadrature (d-q) rotor voltages; φ_{d_st}, φ_{q_st}, φ_{d_r} and φ_{q_r} are the two-phase components in terms of direct and quadrature (d-q) stator and rotor flux linkages; R_r and R_{st} are rotor and stator resistance, respectively; L_m is mutual-inductance; L_{st} is stator-inductance; L_r is rotor-inductance; ω_r and ω represented are the electrical rotor speed and the angular speed. The electrical torque and the equation describing the rotation of the rotor are given in (7).

$$T_e = \left(\frac{3}{2}\right)\left(\frac{P}{2}\right)\left(\lambda_{d\_st} I_{q\_st} - \lambda_{q\_st} I_{d\_st}\right); T_e - T_m = J\frac{d\omega_r}{dt} + B\omega_r \quad (7)$$

Where mechanical torque is denoted as T_m, B is the friction coefficient, and J is the moment of inertia.

On account of the accessibility of the wind energy sources under the cut-in wind velocity and the appearance of rotor friction and losses due to higher wind velocities, a full range of speeds is not presumed for

this study. The range of speed variation is presumed for the study. The rotor speed around the synchronous speed taken for this work is ±10% which is 144 rad/s to 171 rad/s respectively.

$$s = \pm \frac{xR\sqrt{3}V_{dc}}{V_{st}\ 2\sqrt{2}} \tag{8}$$

Where R is the turns ratio of the stator-rotor, x is the modulation index of RSC, V_{dc} is the available voltage at the DCM, and V_{st} is the rated machine voltage. This speed range is computed for the voltage transfer characteristics of RSC [23] as in (8). The wind generator deployed for this work has the ability to deliver power both at the stator and at the rotor, and the total deliverable power is computed as in (9).

$$\left.\begin{aligned} P_{total} &= P_{sp} + P_{rp} = P_{sp} + (1+|s|)\,P_{sp} \\ P_{sp} &= \frac{P_{total}}{(1+|s|)} \\ P_{rp} &= P_{total}\left(\frac{|s|}{1+|s|}\right) \end{aligned}\right\} \tag{9}$$

Where P_{total} indicated is the amount of total power delivered by the DFIG, P_{sp} and P_{rp} are the powers drawn from the stator and rotor, powers. From the design of the speed range, the slip is considered ±0.11 and the rated stator power is 1351.35 W ≈ 1.5 kW.

3.2. Selection of DCM voltage

In order to enable the bidirectional slip power transfer, especially at sub-synchronous speeds, the voltage at the DCM is kept higher than the voltage at the stator end, as in (10) [23].

$$V_{dc} > \frac{3\sqrt{3}V_{st}}{\pi} \tag{10}$$

Where V_{dc} provided is the DC microgrid voltage, and V_{st} stated is the rated stator voltage of DFIG.

3.3. Modeling of RSC

The RSC is a three-phase, bidirectional current-controlled PWM converter, and the current and voltage equations for the above, considering the switching function, are given by (11).

$$\begin{bmatrix} \frac{dI_{d\_r}}{dt} \\ \frac{dI_{q\_r}}{dt} \\ \frac{dV_{dc}}{dt} \end{bmatrix} = \begin{bmatrix} 0 & \omega & \frac{-u_d}{L_f} \\ -\omega & 0 & \frac{-u_q}{L_f} \\ \frac{u_d}{C_{dc}} & \frac{u_q}{C_{dc}} & 0 \end{bmatrix} \begin{bmatrix} I_{d\_r} \\ I_{q\_r} \\ V_{dc} \end{bmatrix} + \begin{bmatrix} \frac{1}{L_f} & 0 & 0 \\ 0 & \frac{1}{L_f} & 0 \\ 0 & 0 & -\frac{1}{C_{dc}} \end{bmatrix} \begin{bmatrix} V_{d\_r} \\ V_{q\_r} \\ I_{dc} \end{bmatrix} \tag{11}$$

Where L_f provided is the line impedance; V_{dc} is the DC microgrid voltage; I_{d_r}, I_{q_r} are the two-phase components in terms of direct and quadrature (d-q) input currents of RSC; I_{dc} indicates the DC side current of RSC; and u_d, u_q are the switching pulses of RSC. The RSC rating that is employed in this work is presumed to be 148.64 W (from (9)).

3.4. Modeling of unbalanced and non-linear loads

The loads applied are three-phase unbalanced and non-linear loads, which have prime practicality status. The three-phase unbalanced resistive loads are assumed to be linear and are modeled as in (12).

$$\left.\begin{aligned} V_{d\_st} &= RI_{d\_stl} \\ V_{q\_st} &= RI_{q\_stl} \end{aligned}\right\} \tag{12}$$

Where R indicates the load component, and V_{d_st}, V_{q_st} are direct and quadrature axes stator voltages. The non-linear load taken for this study is a diode bridge rectifier, with the DC end voltage modeled in (13).

$$V_{dc\_l} = \frac{2*Vst}{\pi} \tag{13}$$

Where V_{dc_l} is the DC side voltage of the non-linear load, and V_{st} is the AC side RMS voltage of the non-linear load.

4. CONTROL METHODOLOGY

4.1. RSC-control method

The decoupled cascaded control scheme for RSC is given in Figure 3(a) and aims at i) reduction of oscillations in electromagnetic torque, stator and rotor powers, ii) regulation of stator voltage and frequency with only one stator parameter, and iii) bidirectional power flow and effective power transfer during multi-modes with flowchart depicted in Figure 3(b).

(a)

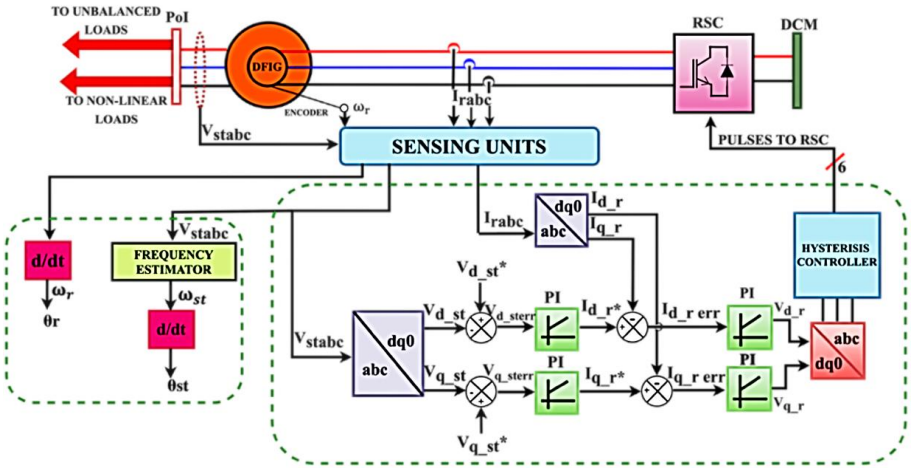

(b)

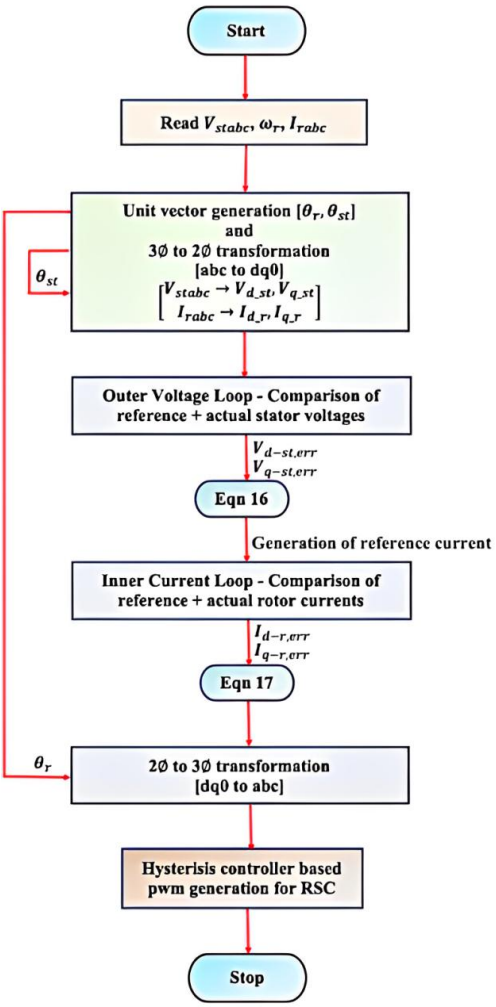

Figure 3. Schematic of (a) current control of RSC and (b) control structure flowchart

A cascaded current control provided in this work initially transforms the three-phase abc quantities to two-phase dq0 quantities to simplify the complexity in control. Also, the unit vectors are computed for the transformation of stator voltage and rotor current using the PLL block, performing as a frequency estimator to provide stator frequency, $\omega_{st,}$ and rotor frequency, $\omega_{r,}$ from the given speed information, respectively. The unit vectors of stator and rotor parameters are θ_{st} and θ_r, and are obtained as in (15).

$$\left.\begin{aligned}\theta_{st} &= \int \omega_{st} dt \\ \theta_r &= \int \omega_r dt\end{aligned}\right\} \quad (15)$$

To simplify system analysis, the three-phase (abc) stator voltages are transformed into a rotating two-axis (dq0) reference frame. Since the control strategy is decoupled, the d- and q-axis components can be regulated independently. The rotating frame stator voltage variables, V_{d_st} and V_{q_st} are compared with reference stator voltage variables, V_{d_st}* and V_{q_st}*. The reference values of d-axis stator voltage variable, V_{d_st}* is set as 0.66 times the required stator phase voltage, whereas the q-axis reference stator voltage, V_{q_st}* is set as V_{q_st}*=0. The PI controller operates on the voltage error in discrete, $G_{\_vs}(Z) = \big(8.24(z-0.02)\big)/(z-1)$ given in (16), bearing minimal loop frequency of about 5Hz and the damping ratio, ζ=0.37. This outer stator voltage loop generates the reference rotor currents, I_{d_r}*, I_{q_r}* so as to deploy in the inner current loop.

$$\begin{aligned} i^*_{d\_r} &= K_{pv}\big(v^*_{d\_st} - v_{d\_st}\big) + K_{iv}\int (v^*_{d\_st} - v_{d\_st})dt \\ i^*_{q\_r} &= K_{pv}\big(v^*_{q\_st} - v_{q\_st}\big) + K_{iv}\int (v^*_{q\_st} - v_{q\_st})dt \end{aligned} \quad (16)$$

The rotor currents in the three-phase abc reference frame are measured from the machine's rotor side and converted into two-phase direct (d) and quadrature (q) components, denoted as, I_{d_r} and I_{q_r}. The d-q rotor voltage components, V_{d_r} and V_{q_r} are controlled to regulate the active and reactive power flow, respectively. The actual and reference rotor currents are compared with the current errors being processed through a discrete PI controller, $G_{\_ir}(Z) = \big(24.1(z-6.2)\big)(z-1)$ as in (17) with a loop frequency of 216 Hz and $\zeta = 0.37$.

$$\begin{aligned} v_{d\_r} &= K_{pi}\big(i^*_{d\_r} - i_{d\_r}\big) + K_{ii}\int (i^*_{d\_r} - i_{d\_r})dt \\ v_{q\_r} &= K_{pi}\big(i^*_{q\_r} - i_{q\_r}\big) + K_{ii}\int (i^*_{q\_r} - i_{q\_r})dt \end{aligned} \quad (17)$$

The rotor voltage components represented in the rotating dq quantities, V_{d_r} and V_{qr} are inversely transformed back into three-phase rotor voltage quantities, V_{rabc} serve as modulating signals at rotor frequency ω_r. The hysteresis controller with a bandwidth of $\pm$0.5 mA processes these modulating signals to produce gate pulses required for switching the rotor side converter.

4.2. Multimode operation

The possible multi-mode operations by the system are formulated, accounting for the various wind/load conditions. Also, the balancing of the power in the system during these operations is maintained through PWM rectification/inversion to have an uninterrupted power supply. The maximum power output corresponding to different rotor speeds under varying wind velocities is estimated using a polynomial curve fitting technique, as described in (18) as referred in [24]. The resulting power curves and the peak power capability of the wind energy system (WES) are illustrated in Figure 4, while the corresponding maximum power values are listed in Table 2.

$$\mathrm{P_{max\_g}} = (0.9)(3.5 - 0.0023\mathrm{N} - 6.3\mathrm{e}^{-6}\mathrm{N}^2 + 0.5\mathrm{e}^{-7}\mathrm{N}^3) \quad (18)$$

Where *N* given is the wind speed. The maximum generated power is delivered to the loads, and the residue of power is fed to DCM to complement other renewable. The different possible operation during the multi-modes is detailed below, and the software selector selects the modes to be executed as depicted in the flow chart (in Figure 5) in the controller.

i) Mode 1: normal operation

The most common mode of wind energy systems is that the load power is less than the generated power $\big[P_{max\_g} > P_{load}\big]$. The machine meets the load demand, and the remaining power $\big(P_{max\_g} - P_{load}\big)$ if available can be used to feed dump loads.

ii) Mode 2: machine stall mode (Pmax_g = 0)

During high/low wind, the turbine blades are locked, then the machine enters stall mode. At this time, the mechanical braking is applied to the system. The critical loads available at the PoI would be supplied by DCM through PWM inversion. The power delivered by the DCM would be negative. A load demand of about 20–30% can be met through this operation, instead of cutting off the supply during this mode.

iii) Mode 3: closed stator [CS]

When an accidental short occurs in the stator, all the windings are presumed to be connected [closed] and the imitating three-phase variable voltage and variable frequency source. Regardless of rotor speed, the RSC undertakes PWM rectification to provide the power generated at the rotor to DCM.

iv) Mode 4: closed rotor [CR]

At times of climatic variations when the wind speed is low, DFIG operates as a cage generator exhibiting a complete three-phase short in the rotor windings. The power generated at the stator, which is a variable voltage/frequency, is supplied to frequency-insensitive loads. During this mode of operation, DFIG is a reactive power load where the external capacitor provides the necessary excitation for the suitable operation in the speed range. The high-frequency harmonics are filtered using the capacitor bank.

Table 2. Maximum power generation

Wind Speed (m/s)	Maximum power P_{max-g} (W)	Speed of Rotor ω_r (rpm)	Wind Speed (m/s)	Maximum power P_{max-g} (W)	Speed of Rotor ω_r (rpm)
3	500	100	8	1350	675
4	750	200	9	1500	800
5	900	275	10	1600	900
6	1150	450	11	1700	1100
7	1200	550			

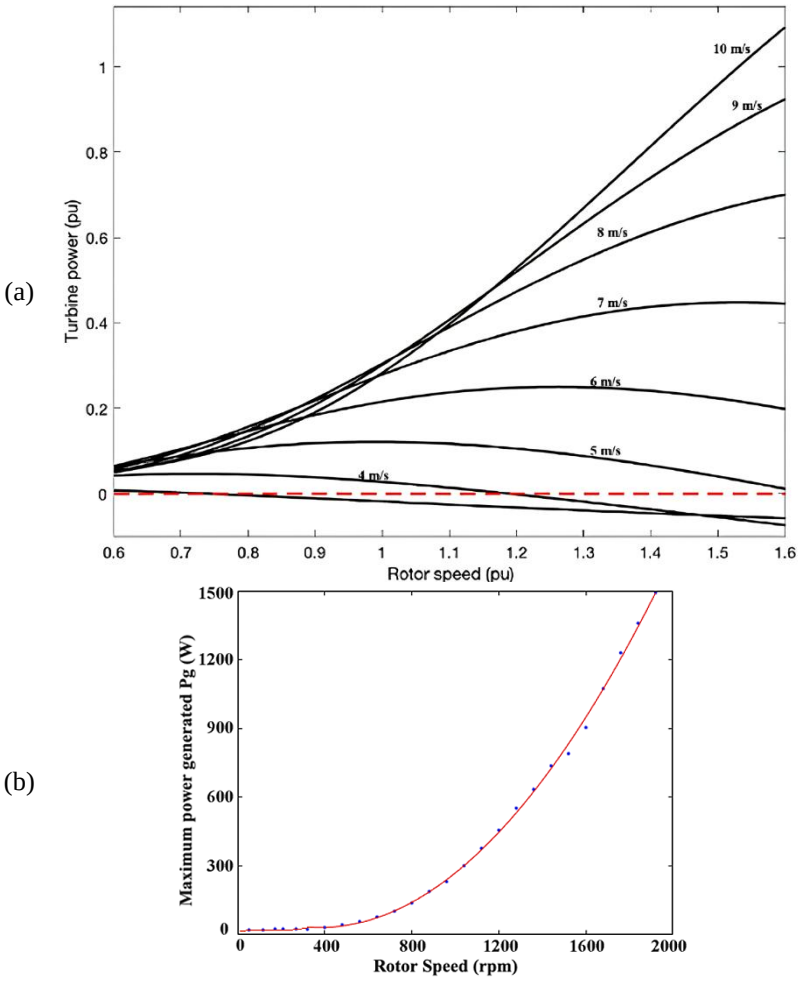

Figure 4. Graphical representation of (a) the turbine power curve and (b) maximum power generation

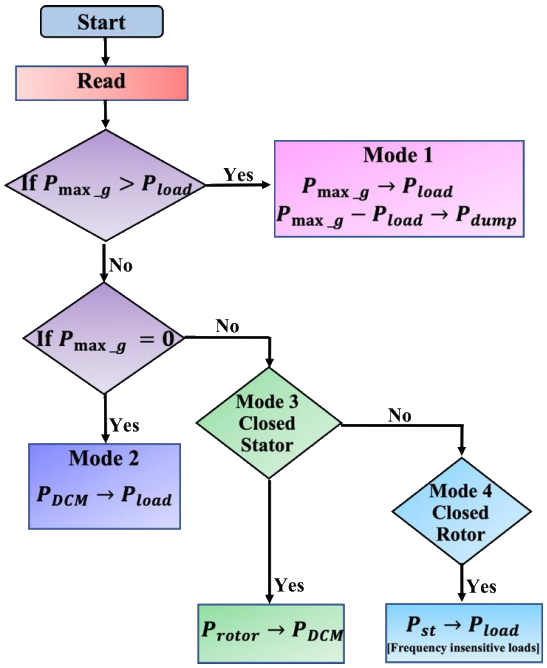

Figure 5. Flowchart for possible operation during the operational modes

5. RESULTS AND DISCUSSIONs – SOFTWARE-In-LOOP (SiL) VALIDATION

A software-in-the-loop (SIL) analysis is carried out to study oscillatory behavior and multi-mode operation of an islanded DFIG-based wind energy system (WES) using the OP4510 real-time digital simulator equipped with eFPGA Sim technology. The experimental setup is configured within RT-Lab, a real-time software environment, which integrates the system model developed using a Master-Slave architecture to validate different operational modes. The host PC operates on an OS capable of executing with a sampling time below 20 μs. Detailed specifications of the OP4510 simulator can be found in [25]. The OP4510 simulator includes the complete system model and necessary signal interfaces to support the control algorithm. Rotor and stator signals, along with the PWM signals for the rotor side converter (RSC), are exchanged in a closed-loop through analog input and output ports 2A and 2B using MATLAB/Simulink R2017b. These signals are output via port 2B and fed back through 2A for pulse generation, enabling real-time execution of the control algorithm based on the operational mode. SIL validation is conducted in extra high performance (XHP) mode, allowing for fast computation. Execution parameters are configured in hardware-synchronized mode to ensure accurate power transfer and effective current control by the RSC. Oscilloscopic verification of results is performed using the DSOX3034T digital storage oscilloscope. Photographic documentation of the experimental setup and the schematic representation of the SIL validation process are presented in Figures 6 and 7, respectively. System specifications are provided in Table 1. The dynamic response of the system during the multimode operations of the system and the presence of oscillations during the presence of unbalance and non-linearity in the system are observed by subjecting the system to speed and load changes. The waveforms are presented with a zoomed view to symbolize the step changes effectively.

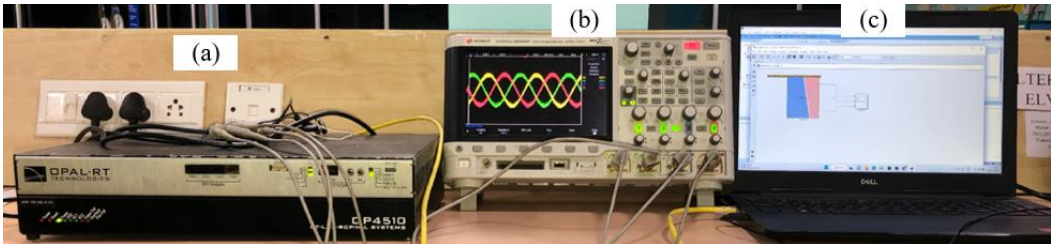

Figure 6. Photograph of the setup: (a) OP4510 RTDS, (b) DSO, and (c) host PC

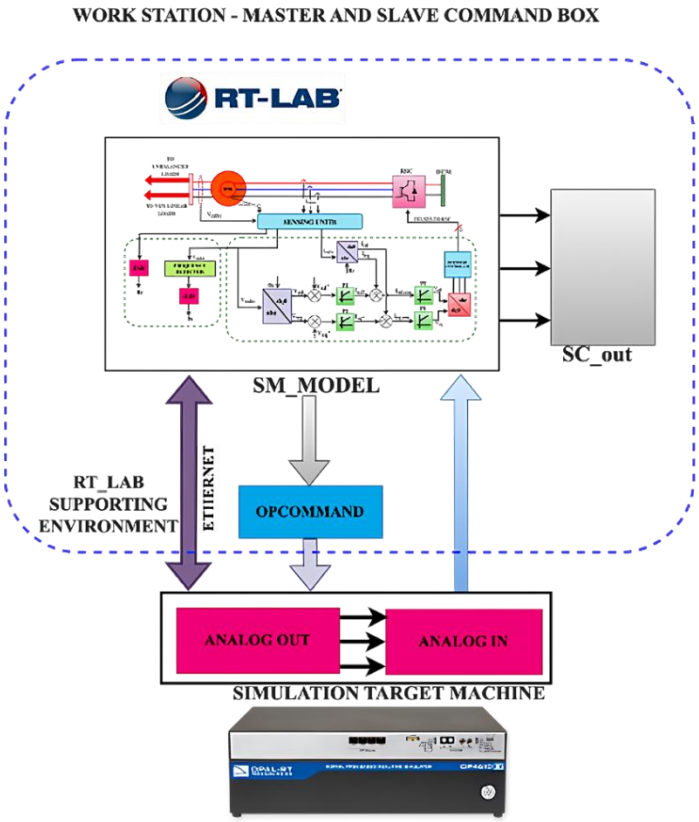

Figure 7. Schematic of SiL validation

5.1. General system performance for speed variations

The performance of the variable speed WES for the variations in speed is evaluated, and the system performance parameters are depicted in Figure 8. The system is loaded with 30% of unbalanced loads, accounting I_{la} = 0.84 A, I_{lb} = 1 A, I_{lc} = 0.9 A. Figures 8(a) and 8(b) show the load currents I_{labc} and the three-phase stator voltages, $V_{sabc,}$ being regulated to 230 V and cycles being 50 Hz in frequency, irrespective of speed change, which is made at instant 't'. Also, during the speed change, which changes from 1380 rpm to 1640 rpm there is no distinct disturbance seen in stator voltage and load currents. Figures 8(c) and 8(d) show the rotor voltages, $V_{rabc,}$ and rotor currents, I_{rabc}. At time instant 't', a change in phase sequence is observed, signifying the bidirectional flow of slip power between the rotor and the DC machine (DCM) during the transition between sub-synchronous and super-synchronous operating modes. Figure 8(e) shows the time domain nature of the RMS stator voltage. The stator voltage is seen to be steady and regulated at 230 V irrespective of speed changes. Also, on account of speed variations at instant 't', the voltage overshoots and settles to a steady value within 500 ms, which is most needed in any WES, as wind is erratic in nature.

5.2. Mode 1: normal operation

The normal operation of WES is such that the generated power would be sufficient for the load power. The dynamic performance is validated with different types of loads: Scenario 1, Scenario 2 – unbalanced load with 30% and 90% loading conditions; and Scenario 3, Scenario 4 – non-linear load with 30% and 90% loading conditions. The unbalanced and non-linear loads exhibit unbalance and non-linearity in the system parameters. In Scenario 1 and Scenario 2, three-phase star-connected unbalanced resistive load with 30% and 90% loading is linked to the PoI with load currents being I_{la} = 0.84 A, I_{lb} = 1 A, I_{lc} = 0.9 A and I_{la} = 2.2 A, I_{lb} = 2.4 A, I_{lc} = 2.3 A, respectively. Figure 9 exhibits the 30% and 90% loading waveforms on the left trace and right trace, respectively. Figure 9(a) depicts the stator voltages being regulated to the rated value of the generator irrespective of the speed change that is initiated at instant 't' from 1380 rpm to 1640 rpm. The power generated, as detailed in section 4.2, varies from 675 to 1000 W with rotor power 100 W and -150 W, respectively. Figure 9(b) depicts the load currents, I_{labc} with respect to the speed change at instant 't'. Figure 9(c) shows the rotor currents, I_{rabc}, and it is found to have oscillations. The power variations for the speed change are observed in Figure 9(d), and the

oscillations are seen as very distinct during 90% loading than during 30% loading. The rotor power and torque oscillations are quantified and detailed in Table 3.

In Scenario 3 and Scenario 4, a 3Ø balanced, non-linear load emulated with an uncontrolled diode bridge rectifier coupled to non-frequency interactive loads with 30% and 90% loading, is presumed to feed load currents are $I_{la} = I_{lb} = I_{lc} = 0.84$ A and $I_{la} = I_{lb} = I_{lc} = 2.6$ A. Figure 10 exhibits the 30% and 90% loading waveforms on the left trace and right trace, respectively. Figure 10(a) depicts the stator voltages being regulated to the rated value irrespective of the speed change made at instant 't'. Figure 10(b) depicts the balanced nonlinear load currents caused due to the 30% and 90% loading. Figure 10(c) shows the rotor currents during 30% and 90% loading conditions. It is observed that the current oscillations are higher during the 90% loading conditions. The power variations with respect to speed changes are shown in Figure 10(d) for 30% and 90% loading, respectively. Similar to the previous two scenarios, the oscillations in rotor current, power, and electromagnetic torque are more pronounced at 90% loading than at 30% loading. The oscillations are quantified and detailed in Table 2.

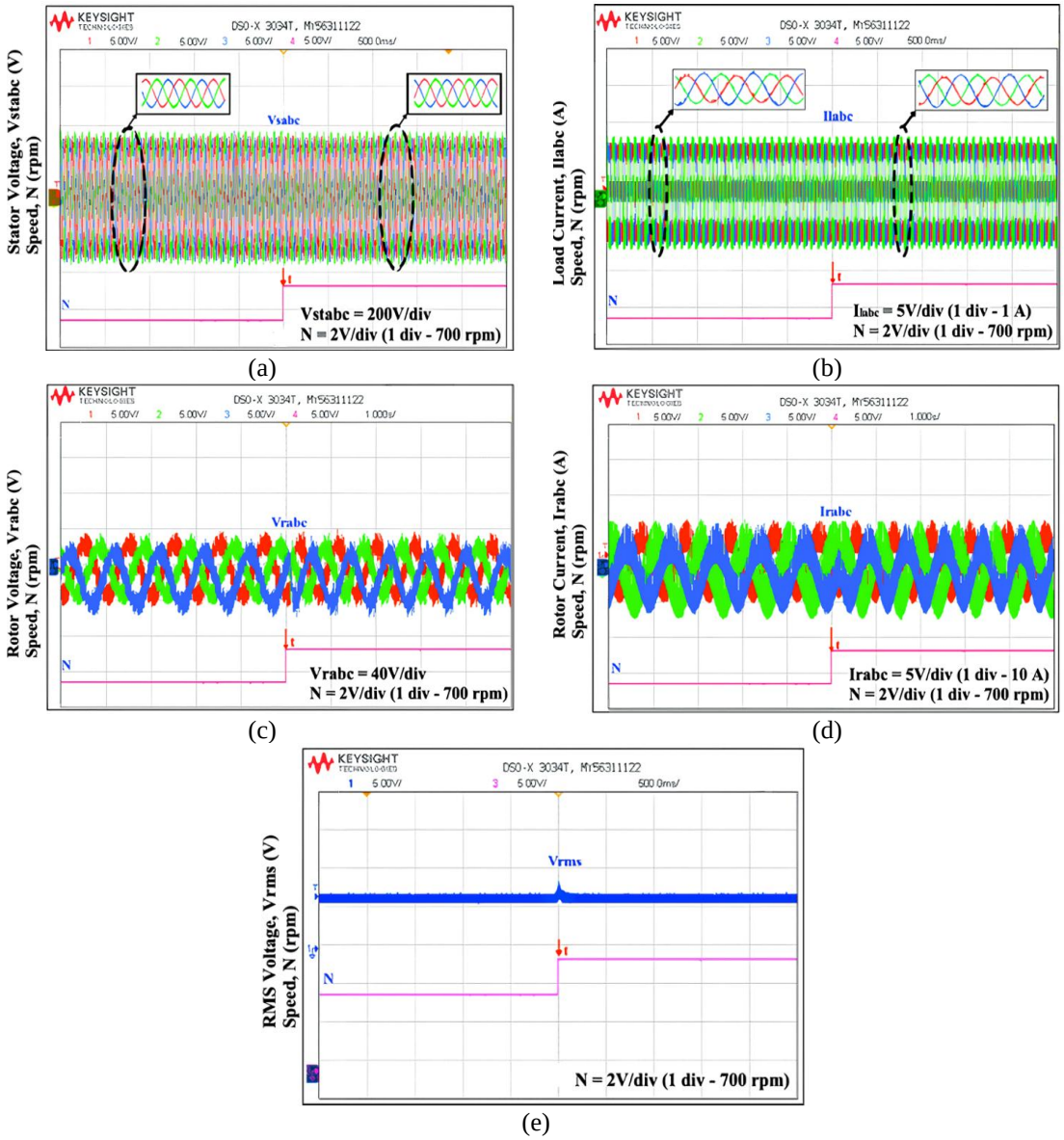

Figure 8. General performance of the system for dynamics in speed: (a) stator voltages with speed, (b) stator currents with speed, (c) rotor voltages with speed, (d) rotor currents with speed, and (e) RMS stator voltage of phase 'a' with speed

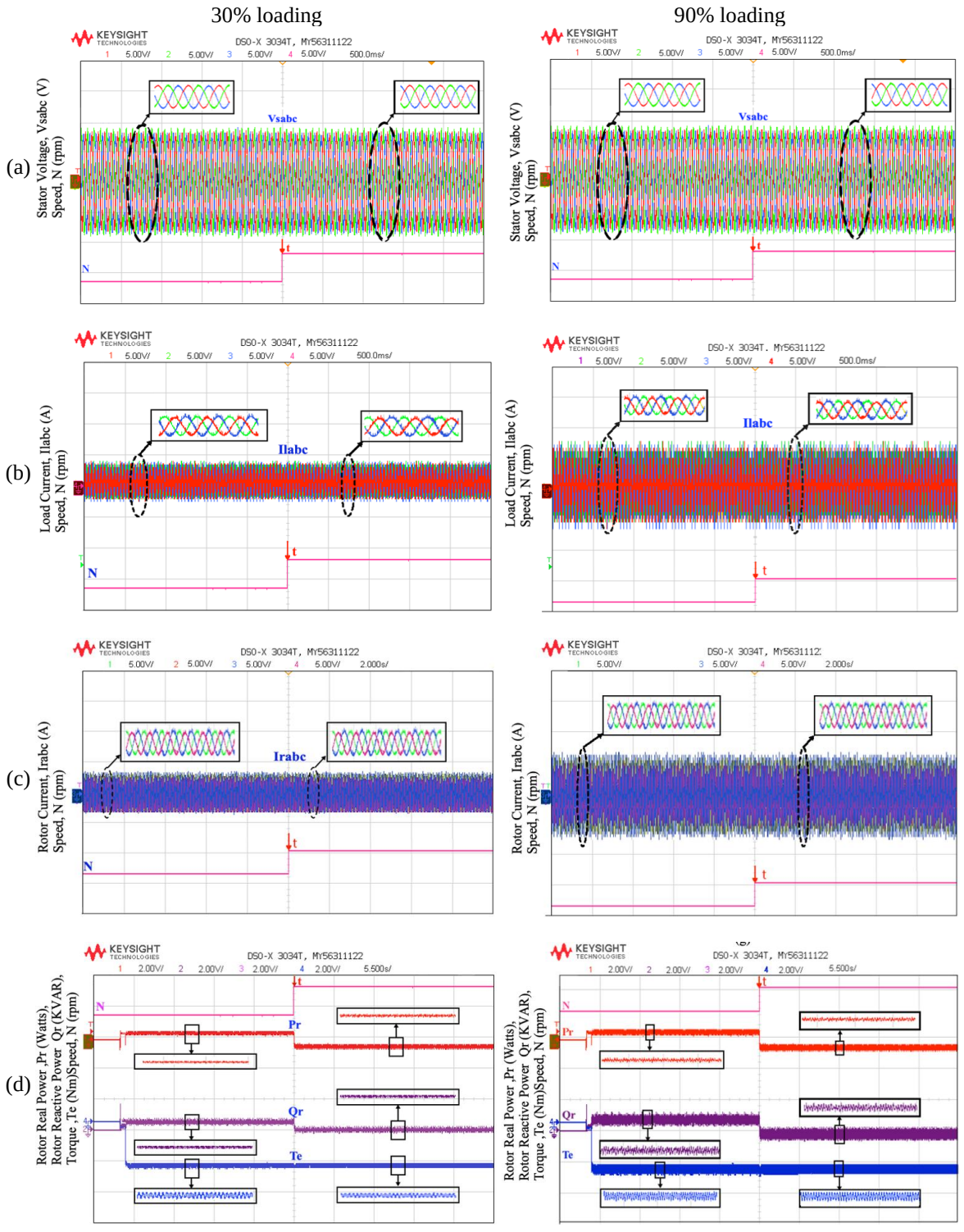

Figure 9. System performance for dynamics in speed with unbalanced loading conditions, where left trace 30% loading and right trace 90% loading: (a) stator voltages with speed; (b) load currents with speed; (c) rotor currents with speed; and (d) rotor real power, rotor reactive power, and torque

The rotor power, torque, and rotor current oscillations during various possible operational modes of the proposed system are tabulated in Table 3, indicating the higher level of oscillations during higher loading and the presence of non-linear loads. Predominantly, the oscillations are observed in the rotor parameters, which would greatly influence the stator parameters, thereby experiencing continued oscillations at the load

end, and the machine will be put under stress and might damage the windings on due course of time of operation. Hence, to avoid the oscillations' effect grid-tied mode can be affected. The rotor currents' THD spectrum for Scenario 2. Scenario 4 is shown in Figures 11(a) and 11(b) respectively, and it is distinct that due at severe oscillations at 90% loading, the non-linearity in the load, it is found that the THD of Scenario 4 is much higher than the THD of Scenario 2.

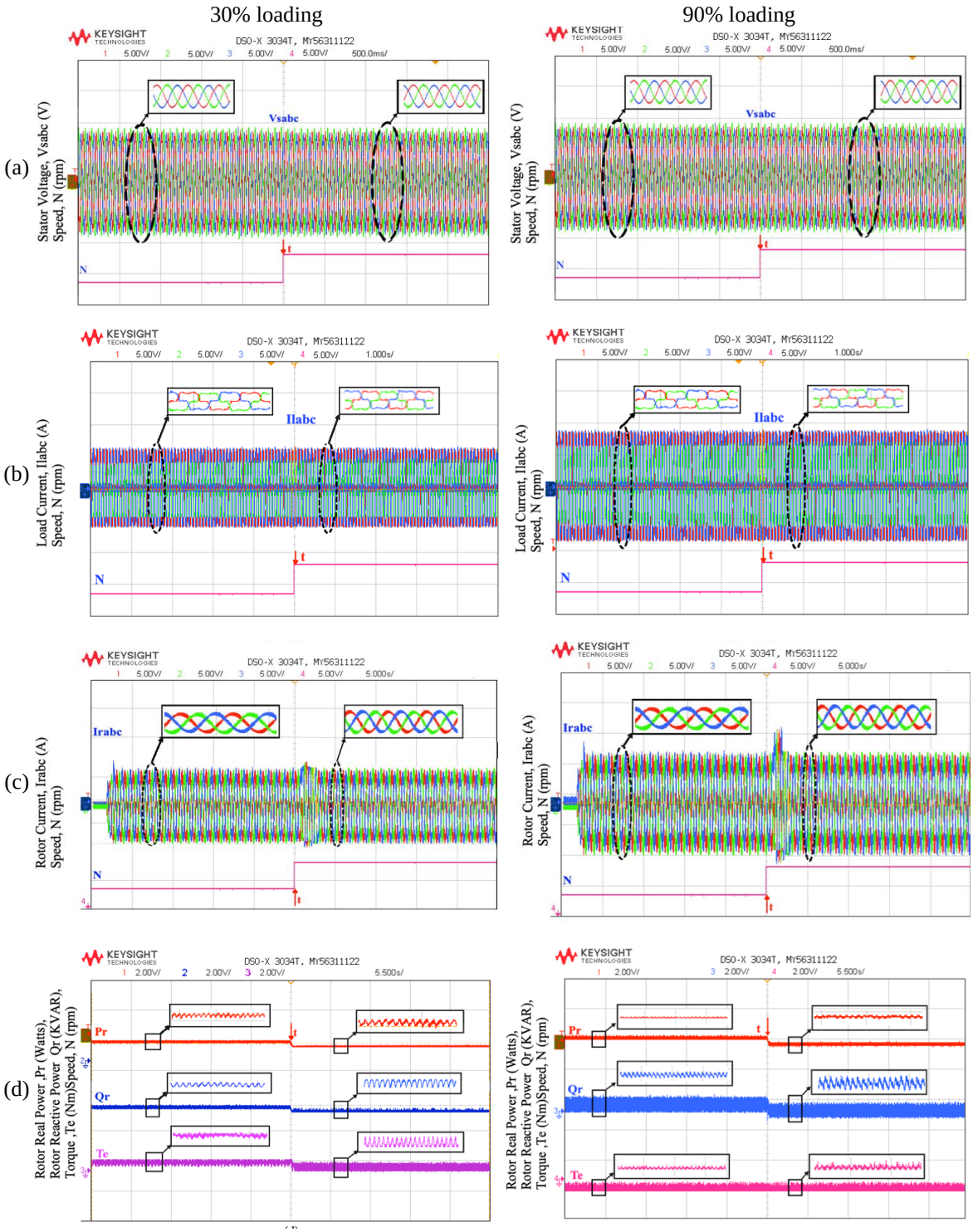

Figure 10. System performance for dynamics in speed with non-linear loading condition, where left trace 30% loading and right trace: 90% loading: (a) stator voltages with speed; (b) load currents with speed; (c) rotor currents with speed; and (d) rotor real power, rotor reactive power, and torque

Table 3. Oscillations observed with unbalanced and non-linear loads

Modes	Load nature	Loading (%)	Te (%)	Ird (%)	Irq (%)	Ps (%)	Qs(%)	Pr (%)	Qr (%)
Mode 1	Unbalanced	30	±6.5	±12.19	±0.25	±6.71	±10	±6.71	±10
[3]	Unbalanced	30	±12.9	ND	ND	ND	ND	±11.42	ND
[4]	Unbalanced	30	±8.0	ND	ND	ND	ND	±13.5	ND
Mode 1	Non-Linear	30	±8.42	±15.33	±0.3	±10.2	±10	±10.2	±10

* T_e – torque, I_{rd} – d components of rotor current, I_{rq} – q axis components of rotor current, P_s – stator real power, Q_s – stator reactive power, P_r – rotor real power, Q_r – rotor reactive power, and *ND* – not discussed

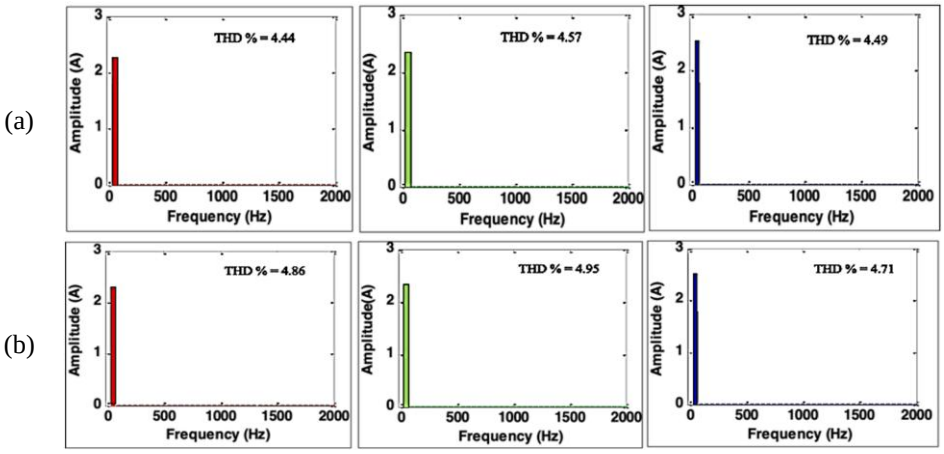

Figure 11. THD spectrum of rotor currents with 90% loading conditions: (a) unbalanced load and (b) non-linear load

5.3. Mode 2: machine stall ($P_{max\_g} = 0$)

In the absence of wind or during the occurrence of a sudden gust of wind impacting the wind blades, mechanical braking is exerted, and the machine is subjected to stall mode with $P_{max\_g} = 0$. The performance is analyzed in this mode, by loading the system with 30% and 90% corresponding to non-linear load with $I_{la} = I_{lb} = I_{lc} = 0.84$ A and $I_{la} = I_{lb} = I_{lc} = 2.6$ A, respectively. The dynamic performance is exhibited in Figure 12. Only critical loads are powered by the DCM through RSC. Figure 12(a), also Figure 12(b) shows 3Ø stator voltages and load currents, respectively. Figures 12(c) shows that the phase 'a' of load voltage and load current are in-phase during 30% and 90% loading. During stall condition, instead of the load being devoid of power, the power from DCM is routed to the loads, thereby providing an uninterrupted power supply.

5.4. Mode 3: closed rotor [CR]

Under uncertain conditions, such as low wind speeds or when the rotor windings experience a short-circuit fault, the wind energy system (WES) operates in a constant reactive (CR) mode, behaving like a real power source combined with a reactive power load. To provide excitation, a capacitor bank is connected to the stator, while the real power generated is supplied to non-frequency-sensitive loads such as heating and lighting. At a specific moment 't', the rotor speed increases from 1380 rpm to 1640 rpm. The waveforms illustrated in Figures 13(a) and 13(b) (see Appendix) represent the stator voltage and current, respectively. The stator current maintains a constant magnitude, whereas the stator voltage changes in response to speed variations, reflecting frequency changes in the stator parameters corresponding to the speed. Figure 13(c) (see Appendix) displays the power fluctuations linked to the speed change at instant 't', showing the real power varying between 300 W and 340 W, and the reactive power ranging from 100 VA to 125 VA.

5.5. Mode 4: closed stator [CS]

The Constant Speed (CS) mode is triggered when a sudden drop in the DC machine (DCM) voltage is detected or when a short circuit occurs in the stator. The dynamic behavior of the wind energy system (WES) under these conditions is illustrated in Figure 14 (see Appendix). With the stator windings shorted, the rotor windings become the primary source of power generation, and the power produced by the rotor is supplied to the DCM, which also provides the necessary excitation to the machine. At instant 't', the speed is varied from 1380 rpm to 1640 rpm, causing corresponding changes in the frequency of the rotor currents and voltages. Figure 13(c) (see Appendix) shows the power transfer during this speed transition, where the real power ranges between 310 W and 370 W, and the reactive power varies from 190 VA to 210 VA.

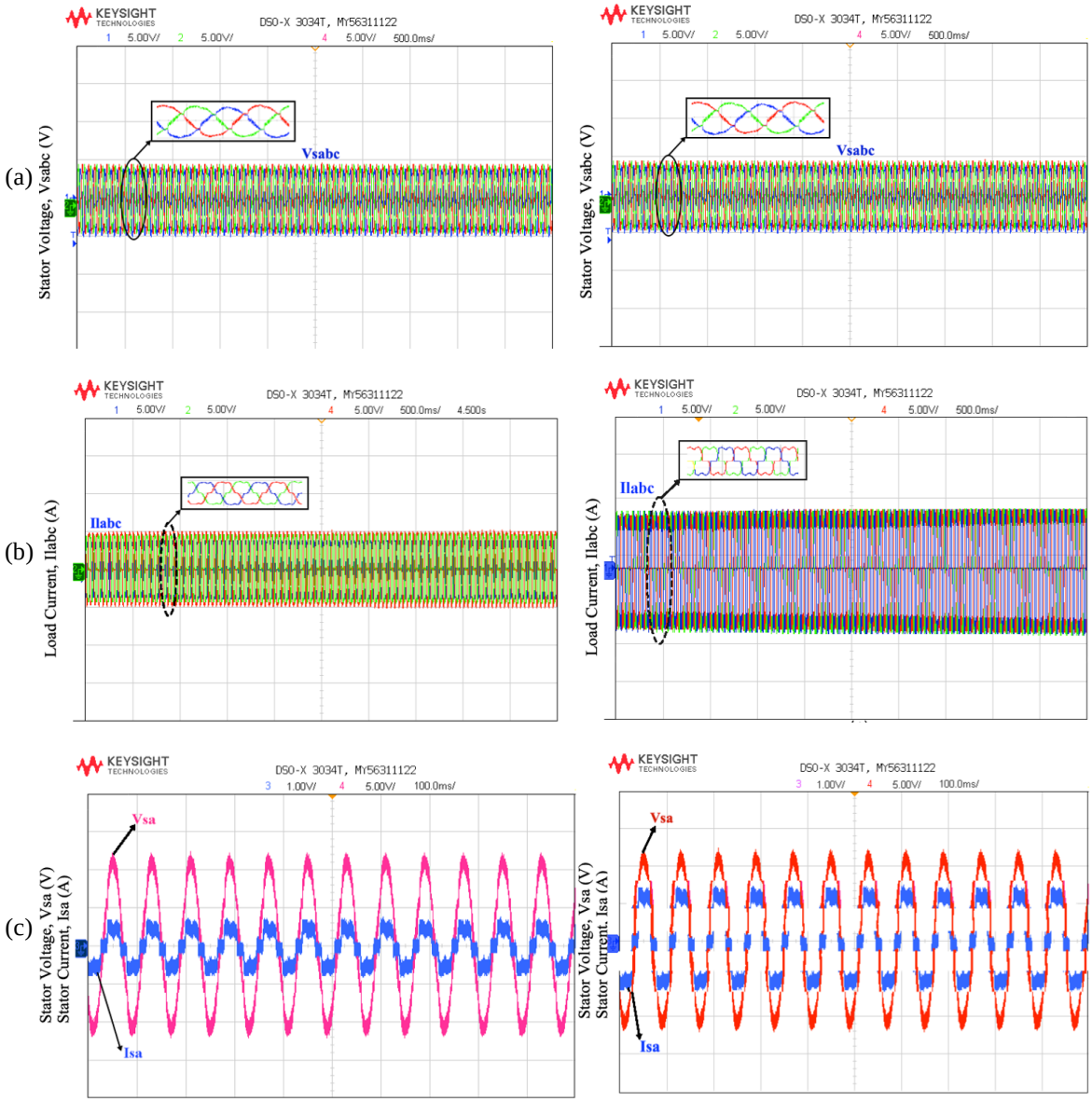

Figure 12. System performance during machine stall condition, where left trace: 30% loading and right trace: 90% loading: (a) stator voltages, (b) load currents, and (c) stator voltage and stator current of 'a' phase

6. CONCLUSION

The power transfer operation and the analysis on the presence of oscillations in variable speed DFIG-based WES operating in islanded mode is reported. All feasible operating modes are developed based on wind speed/load conditions with consideration for occasional scenarios like closed circuit [Closed Stator and Closed Rotor], stall, and normal operation. A cascaded decoupled voltage vector control encompassing an outer voltage loop and delivering the reference for inner current loops is employed in this work for the control of RSC to enable the bidirectional power flow. The RSC regulates the stator parameters and frequency, is accomplished with reduced overshoot during dynamic changes in speed. The system exhibits multi-mode operation, indicating the versatility of the system. All formulated modes and the presence of oscillation accordance to the unbalanced loads [90% loading] ±11.47% T_e, ±13.33% I_{rd}, ±1.3% I_{rq}, ±12.5% P_s, ±15% Q_s, ±12.5% P_r, ±15% Q_r and non-linear loads [90% loading] ±16.6% T_e, ±16.83% I_{rd}, ±1.23% I_{rq}, ±22.6% P_s, ±15% Q_s, ±20.06% P_r, ±15% Q_r are scrutinized through Software-In-Loop (SIL) approach. The SIL results depict the efficacious working of the WES during the multi-mode operation, executing a balance between the various power parameters of the system. Also, it is observed that the system can operate for an extensive speed

range and also on rare occasional modes, exhibiting its versatility with THD values as per IEEE 519 standards. Although the proposed work claims the effective power transfer, it is observed that the system also exhibits oscillations on the rotor power, rotor currents, and torque which might reflect on the stator side leading to stress on the machine and necessitating the grid connection for the system.

FUNDING INFORMATION

The authors would also like to acknowledge the support extended through DST-AISTDF (CRD/2022/000669) and also would like to acknowledge the Measurements and Control Lab, SRM Institute of Science and Technology, Kattankulathur, Chennai, India

AUTHOR CONTRIBUTIONS STATEMENT

This journal uses the Contributor Roles Taxonomy (CRediT) to recognize individual author contributions, reduce authorship disputes, and facilitate collaboration.

Name of Author	C	M	So	Va	Fo	I	R	D	O	E	Vi	Su	P	Fu
P. Preethi Santhosam		✓	✓	✓	✓		✓	✓	✓		✓			
U. Sowmmiya	✓	✓	✓	✓		✓	✓	✓		✓	✓	✓	✓	✓
Tole Sutikno			✓	✓	✓		✓	✓		✓		✓	✓	✓

C : **C**onceptualization
M : **M**ethodology
So : **So**ftware
Va : **Va**lidation
Fo : **Fo**rmal analysis
I : **I**nvestigation
R : **R**esources
D : **D**ata Curation
O : Writing - **O**riginal Draft
E : Writing - Review & **E**diting
Vi : **Vi**sualization
Su : **Su**pervision
P : **P**roject administration
Fu : **Fu**nding acquisition

CONFLICT OF INTEREST STATEMENT

The authors confirm that they have no conflicts of interest to disclose.

DATA AVAILABILITY

Data availability is not applicable to this paper as no new data were created or analyzed in this study.

REFERENCES

[1] F. Kennel, D. Gorges, and S. Liu, "Energy management for smart grids with electric vehicles based on hierarchical MPC," *IEEE Transactions on Industrial Informatics*, vol. 9, no. 3, pp. 1528–1537, Aug. 2013, doi: 10.1109/TII.2012.2228876.

[2] A. Bracale and P. De Falco, "An advanced bayesian method for short-term probabilistic forecasting of the generation of wind power," *Energies*, vol. 8, no. 9, pp. 10293–10314, Sep. 2015, doi: 10.3390/en80910293.

[3] M. Naderi, Y. Khayat, Q. Shafiee, F. Blaabjerg, and H. Bevrani, "Dynamic modeling, stability analysis and control of interconnected microgrids: A review," *Applied Energy*, vol. 334, p. 120647, Mar. 2023, doi: 10.1016/j.apenergy.2023.120647.

[4] Q. Liao, D. Cao, Z. Chen, F. Blaabjerg, and W. Hu, "Probabilistic wind power forecasting for newly-built wind farms based on multi-task Gaussian process method," *Renewable Energy*, vol. 217, p. 119054, Nov. 2023, doi: 10.1016/j.renene.2023.119054.

[5] Y. Wang, Z. Wang, and H. Sheng, "Optimizing wind turbine integration in microgrids through enhanced multi-control of energy storage and micro-resources for enhanced stability," *Journal of Cleaner Production*, vol. 444, p. 140965, Mar. 2024, doi: 10.1016/j.jclepro.2024.140965.

[6] M. A. Asha Rani, C. Nagamani, G. Saravana Ilango, and A. Karthikeyan, "An effective reference generation scheme for DFIG with unbalanced grid voltage," *IEEE Transactions on Sustainable Energy*, vol. 5, no. 3, pp. 1010–1018, Jul. 2014, doi: 10.1109/TSTE.2014.2322672.

[7] C. Nagamani, M. A. Asha Rani, N. Prasannakumar, and A. Karthikeyan, "Reference current generation schemes for DFIG with unbalanced grid voltage," in *2014 IEEE 2nd International Conference on Electrical Energy Systems (ICEES)*, IEEE, Jan. 2014, pp. 65–70. doi: 10.1109/ICEES.2014.6924143.

[8] K. Vijayakumar, N. Kumaresan, and N. Ammasai Gounden, "Operation and closed-loop control of wind-driven stand-alone doubly fed induction generators using a single inverter-battery system," *IET Electric Power Applications*, vol. 6, no. 3, pp. 162–171, Mar. 2012, doi: 10.1049/iet-epa.2011.0204.

[9] R. Datta and V. T. Ranganathan, "Variable-speed wind power generation using doubly fed wound rotor induction machine-a comparison with alternative schemes," *IEEE Transactions on Energy Conversion*, vol. 17, no. 3, pp. 414–421, Sep. 2002, doi: 10.1109/TEC.2002.801993.

[10] J. Hu, H. Nian, H. Xu, and Y. He, "Dynamic modeling and improved control of DFIG under distorted grid voltage conditions," *IEEE Transactions on Energy Conversion*, vol. 26, no. 1, pp. 163–175, Mar. 2011, doi: 10.1109/TEC.2010.2071875.

[11] S. Li, T. A. Haskew, K. A. Williams, and R. P. Swatloski, "Control of DFIG Wind turbine with direct-current vector control configuration," *IEEE Transactions on Sustainable Energy*, vol. 3, no. 1, pp. 1–11, Jan. 2012, doi: 10.1109/TSTE.2011.2167001.

[12] Si Zhe Chen, N. C. Cheung, Ka Chung Wong, and Jie Wu, "Integral sliding-mode direct torque control of doubly-fed induction generators under unbalanced grid voltage," *IEEE Transactions on Energy Conversion*, vol. 25, no. 2, pp. 356–368, Jun. 2010, doi: 10.1109/TEC.2009.2036249.

[13] N. Dahri and M. Ouassaid, "Tracking performance and power quality enhancement of DFIG based wind turbine using robust integral terminal sliding mode control," *e-Prime - Advances in Electrical Engineering, Electronics and Energy*, vol. 10, Dec. 2024, doi: 10.1016/j.prime.2024.100784.
[14] Y. Zhang, J. Hu, and J. Zhu, "Three-vectors-based predictive direct power control of the doubly fed induction generator for wind energy applications," *IEEE Transactions on Power Electronics*, vol. 29, no. 7, pp. 3485–3500, Jul. 2014, doi: 10.1109/TPEL.2013.2282405.
[15] Z. J. Andaloussi, A. Raihani, A. El Magri, and A. Hilali, "Performance improvement of grid-connected wind energy conversion system through definite time horizon control and MPPT based on adaptive observers," *e-Prime - Advances in Electrical Engineering, Electronics and Energy*, vol. 10, p. 100792, Dec. 2024, doi: 10.1016/j.prime.2024.100792.
[16] J. Mohammadi, S. Vaez-Zadeh, S. Afsharnia, and E. Daryabeigi, "A combined vector and direct power control for DFIG-based wind turbines," *IEEE Transactions on Sustainable Energy*, vol. 5, no. 3, pp. 767–775, Jul. 2014, doi: 10.1109/TSTE.2014.2301675.
[17] Yifan Tang and Longya Xu, "A flexible active and reactive power control strategy for a variable speed constant frequency generating system," *IEEE Transactions on Power Electronics*, vol. 10, no. 4, pp. 472–478, Jul. 1995, doi: 10.1109/63.391945.
[18] J. Lee, G. Jang, E. Muljadi, F. Blaabjerg, Z. Chen, and Y. Cheol Kang, "Stable Short-term frequency support using adaptive gains for a DFIG-based wind power plant," *IEEE Transactions on Energy Conversion*, vol. 31, no. 3, pp. 1068–1079, Sep. 2016, doi: 10.1109/TEC.2016.2532366.
[19] M. Mehrasa, E. Pouresmaeil, B. N. Jørgensen, and J. P. S. Catalão, "A control plan for the stable operation of microgrids during grid-connected and islanded modes," *Electric Power Systems Research*, vol. 129, pp. 10–22, Dec. 2015, doi: 10.1016/j.epsr.2015.07.004.
[20] E. Riva Sanseverino, N. Nguyen Quang, M. L. Di Silvestre, J. M. Guerrero, and C. Li, "Optimal power flow in three-phase islanded microgrids with inverter interfaced units," *Electric Power Systems Research*, vol. 123, pp. 48–56, Jun. 2015, doi: 10.1016/j.epsr.2015.01.020.
[21] M. Kumar, S. C. Srivastava, and S. N. Singh, "Control strategies of a DC microgrid for grid connected and islanded operations," *IEEE Transactions on Smart Grid*, vol. 6, no. 4, pp. 1588–1601, Jul. 2015, doi: 10.1109/TSG.2015.2394490.
[22] U. Sowmmiya and U. Govindarajan, "Control and power transfer operation of WRIG-based WECS in a hybrid AC/DC microgrid," *IET Renewable Power Generation*, vol. 12, no. 3, pp. 359–373, Feb. 2018, doi: 10.1049/iet-rpg.2017.0298.
[23] U. Sowmmiya and G. Uma, "Effective performance and power transfer operation of a current controlled WRIG based WES in a hybrid grid," *Renewable Energy*, vol. 101, pp. 1052–1066, Feb. 2017, doi: 10.1016/j.renene.2016.09.068.
[24] R. M. Hilloowala and A. M. Sharaf, "A utility interactive wind energy conversion scheme with an asynchronous DC link using a supplementary control loop," *IEEE Transactions on Energy Conversion*, vol. 9, no. 3, pp. 558–563, Feb. 1994, doi: 10.1109/60.326477.
[25] OPAL RT-Technologies, "OP4510 Simulator," 2015.

APPENDIX

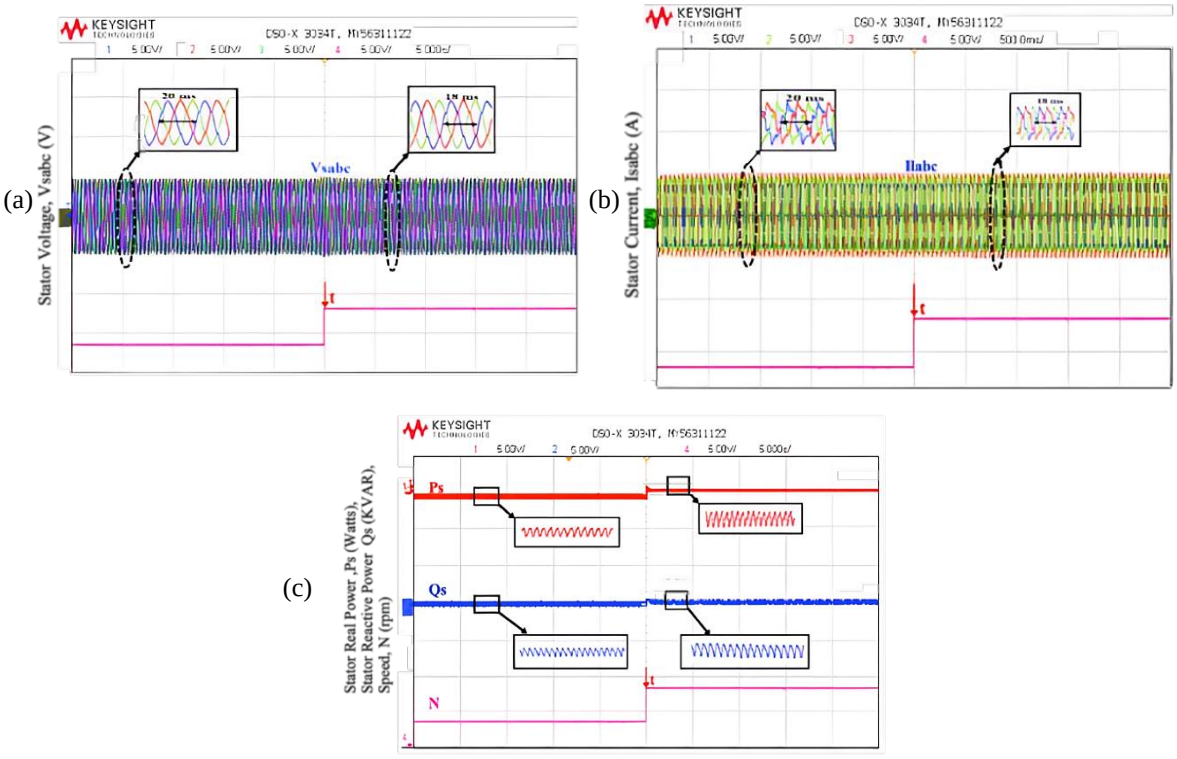

Figure 13. Dynamic performance of the system during closed rotor [CR] with non-linear load: (a) stator voltages with speed, (b) stator currents with speed, and (c) stator real power, stator reactive power with speed

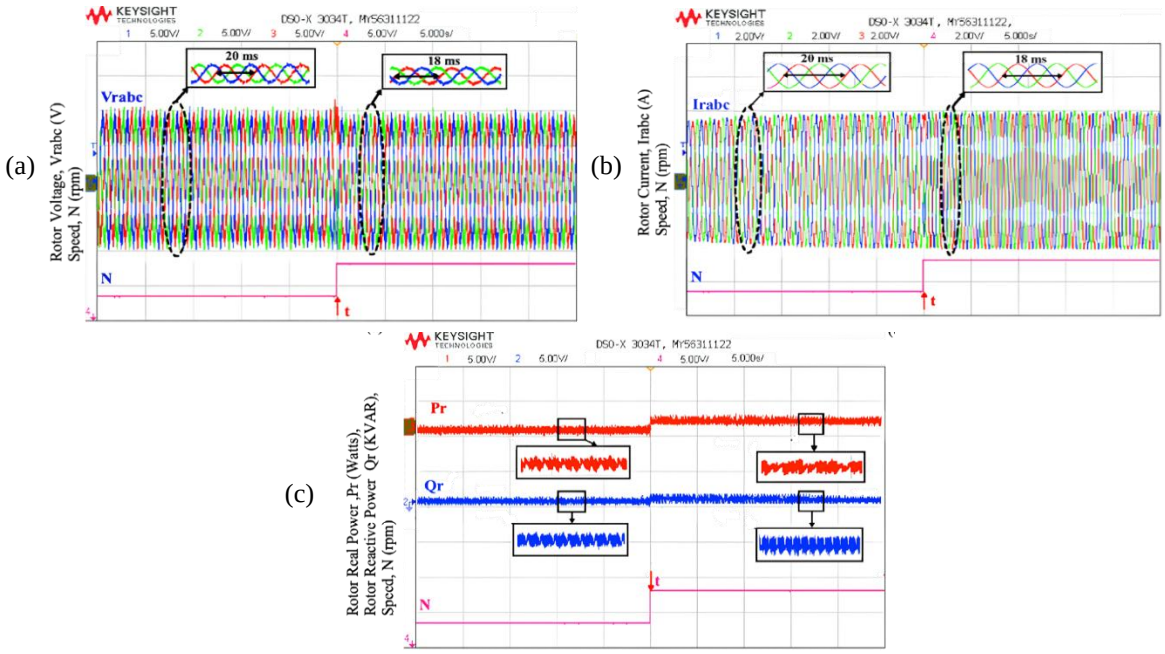

Figure 14. Dynamic performance of the system during closed stator [CR] with non-linear load: (a) rotor voltages with speed, (b) rotor currents with speed, and (c) rotor real power and rotor reactive power with speed

BIOGRAPHIES OF AUTHORS

P. Preethi Santhosam received her B.E. degree in Electrical and Electronics Engineering from Dhanalakshmi College of Engineering, Chennai, India. She obtained her M.E. degree in Power Engineering and Management from the College of Engineering, Guindy, Anna University, Chennai. She is currently pursuing her Ph.D. in the Department of Electrical and Electronics Engineering at SRM Institute of Science and Technology, Kattankulathur, India. Her research interests include control strategies for wind energy conversion systems, standalone and hybrid microgrids, power electronics, and renewable energy integration. She has worked on various real-time implementations using FPGA and OPAL-RT simulators, focusing on rotor-side converter control for doubly fed induction generator (DFIG)-based wind systems. She can be contacted at email: preethisanthosam1803@gmail.com

U. Sowmmiya obtained her B.E. degree in Electrical and Electronics Engineering and M.E. degree with specialization in Power Electronics and Drives from Anna University, Chennai. She also obtained her Ph.D. degree from the College of Engineering, Guindy, Anna University, Chennai. She is awarded a Post-Doctoral Fellowship under the Young Scientist Fellowship Scheme of TNSCST at the National Institute of Technology, Karnataka. Presently, she is working as an Associate Professor in the Electrical and Electronics Engineering Department of SRM Institute of Science and Technology, Kattankulathur. Her current research interests are grid integration of renewable sources, condition monitoring, power transfer in wind energy conversion systems, and power quality issues in propulsion systems. Currently, the ongoing projects investigated by her are funded by MoES, DST, and SRM-SERI. She is a life member of ISTE, a member of IEEE, IEI, IAEMP, and IET. She is also the Branch Counsellor for the SRM-IAEMP Student Chapter. She can be contacted at email: sowmmeee@gmail.com.

Tole Sutikno is a lecturer and the Head of the master's program of Electrical Engineering at the Faculty of Industrial Technology at Universitas Ahmad Dahlan (UAD) in Yogyakarta, Indonesia. He received his Bachelor of Engineering from Universitas Diponegoro in 1999, Master of Engineering from Universitas Gadjah Mada in 2004, and Doctor of Philosophy in Electrical Engineering from Universiti Teknologi Malaysia in 2016. All three degrees are in Electrical Engineering. He has been a Professor at UAD in Yogyakarta, Indonesia, since July 2023, following his tenure as an associate professor in June 2008. He is the Editor-in-Chief of TELKOMNIKA and head of the Embedded Systems and Power Electronics Research Group (ESPERG). He is one of the top 2% of researchers worldwide, according to Stanford University and Elsevier BV's list of the most influential scientists from 2021 to the present. His research interests cover digital design, industrial applications, industrial electronics, industrial informatics, power electronics, motor drives, renewable energy, FPGA applications, embedded systems, artificial intelligence, intelligent control, digital libraries, and information technology. He can be contacted at email: tole@te.uad.ac.id.